AN INVESTIGATION OF BOILING PROCESSES IN HYDROTHERMAL ERUPTIONS

T.A. SMITH & R. McKIBBIN

Institute of Fundamental Sciences-Mathematics, Massey University

SUMMARY - Development of mathematical models for hydrothermal eruptions depends crucially on understanding transient boiling processes in porous media. Physical and numerical experiments are currently being carried out to investigate the progression of boiling fronts through porous media. Observations from a laboratory eruption support our conceptual model for hydrothermal eruptions. Observations from another laboratory experiment, a numerical experiment using a mathematical model based on conservation laws, and computer simulations are compared. While qualitative results for these models are similar, more investigation is needed to obtain quantitative agreement.

1. INTRODUCTION

Hydrothermal eruptions are violent events which eject a mixture of water, steam and rock particles without warning. Though rare temporally, many have occurred in geothermal fields in New Zealand, as well as around the world.

A summary of previous work on the modeling of hydrothermal eruptions and a conceptual model describing the eruption process can be found in Smith & McKibbin (1997). The conservation equations and boundary conditions describing the flow in hydrothermal eruptions are outlined in Smith & McKibbin (1998).

In this paper we continue our investigation on the modeling of hydrothermal eruptions, focusing on the process which drives the eruption, the boiling of hot groundwater. The behavior of the *boiling front* as it moves through the porous medium is investigated through both physical and numerical experiments.

2. LABORATORY ERUPTION

It has been hypothesized that hydrothermal eruptions occur due to a sudden pressure reduction at the surface. A depressurization of fluid would initiate boiling at the surface and a boiling front would then progress downward through the porous medium. A laboratory model of a hydrothermal eruption has been constructed to test the validity of this proposed triggering mechanism and to provide visual observations of the processes which occur during an eruption.

In this model (see Figure 1), a Pyrex cylinder was filled with sand and the sand was saturated with liquid water. The column was then heated to near 100°C and connected to a Pyrex catch basin. This basin was designed to act as a receiver for erupted material and to provide ambient conditions for the eruption. With the use of a vacuum pump, the pressure in the basin was reduced to boiling point conditions. This allowed boiling to begin at the top of the eruption column triggering the laboratory hydrothermal eruption. A boiling front was initiated at the surface, sand was thrown from the top of the eruption column and the boiling front quickly progressed downwards through the column. Two seconds after the eruption began, the boiling front had moved through more than half of the column [see arrow in Figure 2 (b)]. Small gaps could be seen in the sand produced by the boiling of water and the upward movement of the sand. After seven seconds the eruption was at its height. The boiling front had progressed completely through the eruption column and larger gaps were formed [see Figure 2 (c)]. After this point, the eruption slowed and eventually stopped. Some slumping occurred as material fell back down the eruption column [see Figure 2(d)].

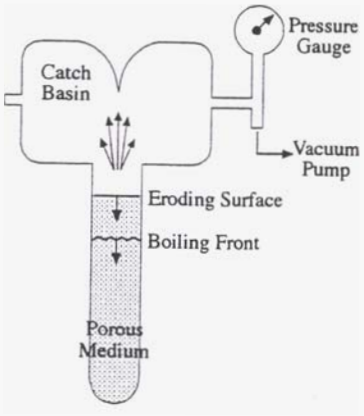

Figure 1. Laboratory hydrothermal eruption.

This first model supports the hypothesis that a pressure reduction at the surface may trigger an eruption and initiate a downwards-moving boiling front. Physical features observed in naturally-occurring hydrothermal eruptions, including the

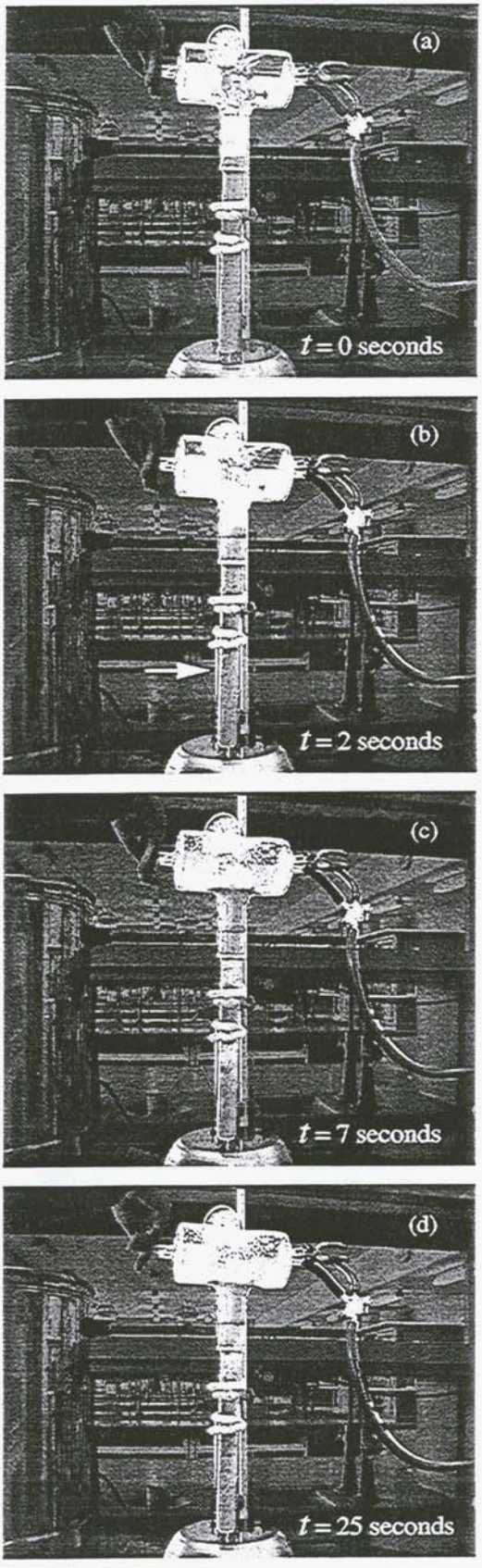

Figure 2. Laboratory hydrothermal eruption in progress.

ejection of solid material and ground slumping following an eruption (see Allis, **1984),** were also observed. Improvements in design are planned and it is hoped that future models may provide us with estimates of the rate at which material is ejected from the eruption column and of the speed at which the boiling front moves through the porous medium. Such quantitative information may then be integrated with information from the literature on natural hydrothermal eruptions and numerical data from mathematical models to provide a more complete picture of the processes involved.

3. BOILING IN POROUS MEDIA: NUMERICAL EXPERIMENT

In modeling hydrothermal eruptions, the principles of conservation of mass, momentum and energy are used to formulate the mathematical problem. **A** set of non-linear partial differential equations governing the transient mass and energy transport have been obtained (see Smith and McKibbin, **1998).**

In this section we look at the simpler case of solving these equations in one horizontal dimension. A one-dimensional core of semi-infinite length is initially saturated with liquid water and is at some constant pressure throughout. If, **as** in the case of the hydrothermal eruption, the pressure is then reduced at one end of the porous medium, the pressure reduction will cause boiling to occur and flow to commence. A boiling front will be initiated at the end of the core and will quickly progress through the porous medium.

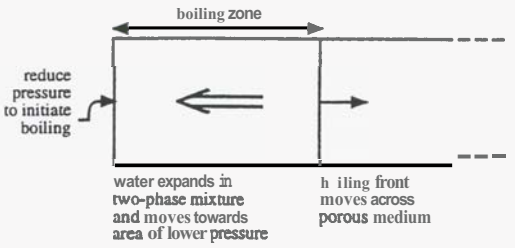

Figure 3. Schematic of boiling front propagation in a porous medium.

We present here two models for this fluid flow. In forming our models, we consider a small representative elementary volume taken from the porous media which is large enough to contain both some rock and some fluid, but is small enough that the density of the water mixture in the volume is uniform throughout. In our first model, we assume that because of the rapidity of motion, a separable two-phase flow does not have time to develop. Therefore, the fluid is considered to be a homogeneous mixture of liquid water and water vapor. In the second model, the water mixture is modeled **as** two separate phases.

In both models, the conservation of mass and energy equations can be written respectively as follows

$$\frac{\partial A_m}{\partial t} = -\frac{\partial \mathbf{Q}_m}{\partial x} \tag{1}$$

$$\frac{\partial A_e}{\partial t} = -\frac{\partial \mathbf{Q}_e}{\partial x} \tag{2}$$

where A_m and A_e are the fluid mass and energy per unit volume of formation and $\mathbf{Q}_m$ and $\mathbf{Q}_e$ are the mass and energy fluxes per unit area. The time t is taken to be zero at the moment the end of the core is depressurized and the positive distance x is measured from this end of the core.

Expressions for A_m, A_e, $\mathbf{Q}_m$, and $\mathbf{Q}_e$ in terms of matrix and fluid parameters are given in Section 3.1 for the homogeneous mixture flow case and in Section 3.2 for the separable-phase flow case. In both cases, Equation (1) states that the time rate of increase of mass inside a representative elementary volume equals the mass flow rate across the surface of the volume, while Equation (2) states that the change in energy inside the volume is equal to the advected energy flow rate across the surface plus the energy gained or lost by conduction.

3.1 Homogeneous Mixture (HM) Flow Model

In the case of the homogeneous mixture model, a single-phase Darcy's Law with parameters that depend on the two-phase fluid mixture is used in describing the mass flow rate per unit area. Under this assumption we have

$$A_m = \phi \rho_f \tag{3}$$

$$A_e = (1-\phi)\rho_r c_r T_{sat} + \phi \rho_f u_f \tag{4}$$

$$\mathbf{Q}_m = k\frac{\rho_f}{\mu_f}\left(-\frac{\partial p}{\partial x}\right) \tag{5}$$

$$\mathbf{Q}_e = h_f \mathbf{Q}_m + K\left(-\frac{\partial T_{sat}}{\partial x}\right) \tag{6}$$

Here the subscript f is used to represent the fluid mixture and the subscript r represents the rock matrix. The rock properties are assumed to be constant and are as follows: ϕ is the porosity, k is the permeability, c_r is the matrix heat capacity, K is the thermal conductivity, and ρ_r is the rock density. The properties of the fluid are: ρ_f is the fluid density, μ_f is the dynamic viscosity, h_f is the specific enthalpy, and u_f is the specific internal energy. $T_{sat}(p)$ is the saturation temperature, the temperature at which water boils for a given pressure p. Alternatively, for a given temperature T, $p_{sat}(T)$ is the saturation pressure. At such so-called saturated conditions, both liquid water and water vapor may be present in the system. Saturation temperature increases with increasing pressure (see for example any standard set of steam tables).

Note that the model assumes that, by Darcy's Law, the mass flow rate Q, is proportional to the dynamic pressure gradient. Fluid flows towards areas of lower pressure.

The density, dynamic viscosity and specific enthalpy of the two-phase fluid mixture are given by

$$\rho_f = S\rho_l + (1-S)\rho_g \tag{7}$$

$$\mu_f = S\mu_l + (1-S)\mu_g \tag{8}$$

$$h_f = \frac{S\rho_l h_l + (1-S)\rho_g h_g}{\rho_f} \tag{9}$$

$$u_f = Su_l + (1-S)u_g \tag{10}$$

where S is the liquid saturation (volume fraction of fluid that is liquid) and the subscripts l and g generally refer to the liquid and gas phases.

The fluid is at saturated (boiling) conditions, and standard correlations for the thermodynamic properties of water may be used.

The expressions (3)– (10) are substituted into the conservation of mass and energy equations (1) and (2), to give:

$$A_1 p_t + B_1 S_t = C_1 p_x S_x + D_1 (p_x)^2 + E_1 p_{xx} \tag{11}$$

$$A_2 p_t + B_2 S_t = C_2 p_x S_x + D_2 (p_x)^2 + E_2 p_{xx} \tag{12}$$

where the coefficients A_1, A_2, B_1, B_2, C_1, C_2, D_1, D_2, E_1, and E_2 are (non-linear) functions of pressure and saturation, and the subscripts x and t are used to represent the partial derivatives with respect to x and t respectively.

Equations (11) and (12) may then be reduced to a simpler set of ordinary differential equations by use of the similarity variable $\eta = x/\sqrt{t}$.

$$\frac{1}{2}\eta A_1 p' + \frac{1}{2}\eta B_1 S' = C_1 p' S' + D_1 (p')^2 + E_1 p'' \tag{13}$$

$$\frac{1}{2}\eta A_2 p' + \frac{1}{2}\eta B_2 S' = C_2 p' S' + D_2 (p')^2 + E_2 p'' \tag{14}$$

Here the superscripts ' and '' are used to represent the first and second derivatives with respect to η.

The core is assumed to be initially saturated with liquid water and at some pressure $p = p_{initial}$. At time $t = 0$, the pressure at one end of the core (denoted $x = 0$) is reduced to $p = p_{final}$. Therefore, at $t = 0$ or as x tends to infinity (both equivalent to η tending to infinity), we have $S = 1$, $p = p_{initial}$, and $p' = 0$. At $x = 0$ or as t tends to infinity (equivalent to $\eta = 0$), $S = S_{final}$, $p = p_{final}$, and $p' = p'_{final}$. S_{final} and p'_{final} are unknown, but may be found using a shooting method.

Under these boundary conditions, Equations (13) and (14) can be solved numerically to obtain liquid saturation and pressure distributions along the porous medium sample, providing a description of the progression of the boiling front as it moves through the porous medium.

3.2 Separable Phase (SP) Flow Model

In the case of separable phase flow, a two-phase Darcy Law is used in determining the mass flow rate per unit area. The fluid mass and energy per unit volume of formation and mass and energy fluxes per unit area in this case are given by

$$A_m = \phi\left[S\rho_l + (1-S)\rho_g\right] \tag{15}$$

$$A_e = (1-\phi)\rho_r c_r T_{sat} + \phi\left[S\rho_l u_l + (1-S)\rho_g u_g\right] \tag{16}$$

$$Q_m = k\left(k_{rl}\frac{\rho_l}{\mu_l} + k_{rg}\frac{\rho_g}{\mu_g}\right)\left(-\frac{\partial p}{\partial x}\right) \tag{17}$$

$$Q_e = k\left(k_{rl}h_l\frac{\rho_l}{\mu_l} + k_{rg}h_g\frac{\rho_g}{\mu_g}\right)\left(-\frac{\partial p}{\partial x}\right) + K\left(-\frac{\partial T_{sat}}{\partial x}\right) \tag{18}$$

In a similar manner to the solution of the HM flow case, the conservation of mass and energy equations given in (1) and (2) can be combined with Equations (15) - (18) and re-written in the form of Equations (11) and (12). In this case the coefficients $A_1, A_2, B_1, B_2, C_1, C_2, D_1, D_2$, E_1 and E_2 are again (non-linear) functions of pressure and saturation, but they are different from those used in the homogeneous mixture case. The similarity variable η is again used to write the conservation of mass and energy equations in the form of (13) and (14) and these equations are then solved numerically using the same boundary conditions given in Section 3.1.

3.3 Comparison of HM and SP Model Results

A comparison of calculated solutions for the homogeneous mixture flow model with those for the separable phase flow model shows that for a given pressure reduction at one end of a porous medium sample, more liquid water is predicted to be converted to gas in the HM case than in the SP case. It is also predicted that the boiling front progresses at a faster rate in the SP case than in the HM case.

This is illustrated in the following example. Consider a porous medium sample with $\phi = 0.18$, $k = 10^{-10}\,m^2$, $c_r = 1000$ J/kgK, $K = 2$ W/mK and $\rho_r = 2650$ kg/m^3. Assume that the sample is initially at a pressure $p_{initial} = 1.1$ bar and temperature $T = T_{sat}(p) = 102.3$ °C; the pressure at one end of the sample is suddenly reduced to $p_{final} = 1$ bar. In the HM case **95%** of the liquid water in the core is converted to water vapor, to give $S_{final} = 0.05$. In the SP case only **58%** is converted ($S_{final} = 0.42$). It can also be shown that in the HM case it would take about 22 seconds for the boiling front to progress through 1 m of the core, while in the SP case it would take about 12 seconds to travel this same distance. Saturation and pressure distributions for the two cases are shown in Figure 4.

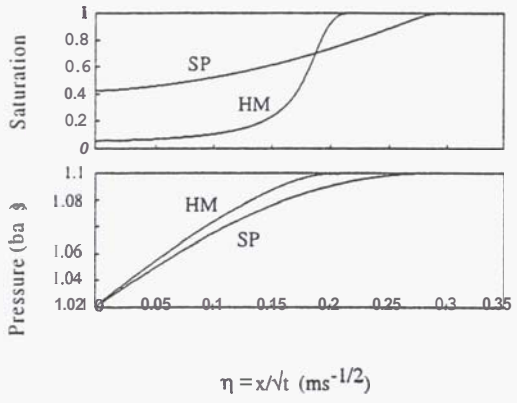

Figure 4. Saturation and pressure distributions in a one-dimensional horizontal porous medium sample.

4. BOILING IN POROUS MEDIA: PHYSICAL EXPERIMENT

This section reports on a physical experiment on rapid transient boiling in porous media, intended to provide data to be used to test the validity or otherwise of the mathematical models described in Section 3. Results provided are preliminary and allow a qualitative comparison only.

In this physical experiment, a porous medium sample is placed inside a containment vessel. The sample is then saturated with liquid water. A decrease in pressure at one end of the sample allows boiling to occur. A boiling front is initiated at the end of the vessel and quickly moves through the sample (see Figure 3). Nuclear Magnetic Resonance techniques are used to image the liquid water content throughout the

sample over time, providing a picture of the progression of the boiling front as it moves through the core.

4.1 Apparatus and Procedure

The experimental apparatus consists of a containment vessel, connection hose, ambient condition reservoir, Nuclear Magnetic Resonance (NMR) equipment and a vacuum pump (see Figure *5).*

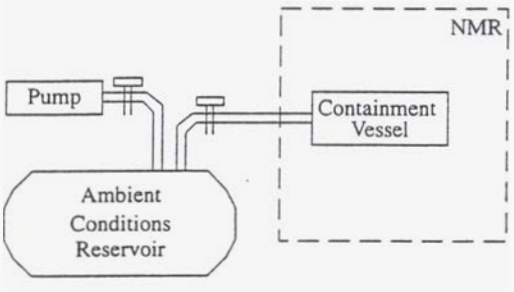

Figure 5. Experimental apparatus.

In the experiment, a cylindrical rock core was sealed around its sides and one end. Its other end remained open to allow the eventual flow of fluid from the rock to the ambient condition reservoir. The core was initially saturated with de-ionized water and its dimensions, average porosity, permeability (from a permeameter experiment) and density were calculated.

A cylindrical brass chamber, 3 litres in volume, was used to provide "ambient" conditions for the experiment. Most of the air was removed fiom the reservoir enabling the pressure within the reservoir to be controlled by the temperature. [An addition of a small amount of water into the reservoir would then provide an ambient pressure of $p_{air} + p_{sat}(T_{ambient})$.] The temperature of the reservoir was reduced to $T_{ambient}$, a temperature low enough to provide ambient pressure conditions which would initiate boiling in the core.

A hose, diameter 8 mm and length 2.5 m, was filled with cold water and used to connect the ambient condition reservoir to the core. The core was placed inside the NMR, the vacuum pump was turned off and the initial pressure p_{air} and temperature $T_{ambient}$ inside the reservoir were recorded.

The experiment was initiated by opening the tap between the reservoir and the connecting hose. The cold water inside the hose boiled due to the pressure reduction and flowed into the ambient condition reservoir. The addition of this water to the reservoir provided the ambient pressure for the experiment of $p_{air} + p_{sat}(T_{ambient})$.

Shortly after the opening of the tap, boiling was initiated at the depressurized end of the core and the NMR equipment was used to measure the spatially-distributed image of water concentration in the core.

4.2 Results

A number of laboratory experiments were performed using a bentheimer rock core of length 12.5 cm and diameter 3.8 cm. Approximate rock properties were: $\rho_r = 2000$ kg/m^3, $\phi = 0.18$, $K = 2$ W/mK, $c_r = 1000$ J/kg, and $k = 10^{-12}$ m^2. The initial temperature and pressure inside the ambient condition reservoir were $T_{ambient} = 2$ °C and $p_{air} = 5$ mbar providing an ambient pressure for the experiments of approximately $p_{air} + p_{sat}(T_{ambient}) = 12$ mbar.

Using NMR imaging, one-dimensional liquid saturation distributions along the core were found. Some NMR images are reproduced here with comments.

Experiment A: The core was initially at atmospheric conditions (approximately 1 bar and 20 °C) and saturation distributions were found every 200 milliseconds for 25 seconds. Two measured saturation distributions are shown in Figure 6.

We have assumed the core was initially saturated with liquid water. An image of liquid saturation was taken before boiling was initiated and subsequent images have been normalized with respect to this initial distribution.

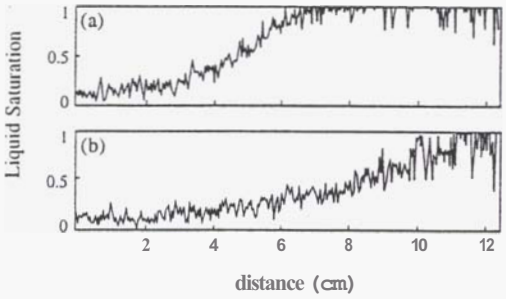

Figure 6. Experiment A. Two images of liquid saturation: image (a) was taken within 200 milliseconds of the onset of boiling, and image (b) a further 200 milliseconds later.

While data obtained shows a boiling front moving through the core as expected, the progression of the front occurs quickly and not enough information about the process is obtained. In less than 200 milliseconds [see Figure 6 (a)] boiling has apparently begun in the first 7 cm of the core, while in fewer than 400 milliseconds [see Figure 6 (b)] boiling is occurring throughout the core. According to numerical results, this process should occur at a much slower rate.

Experiment B: The core was again initially at atmospheric conditions. Saturation images in

this case were found every half-second for 10 minutes. Three saturation distributions obtained are shown in Figure 7. Again, distributions have been normalized with respect to an initial scan.

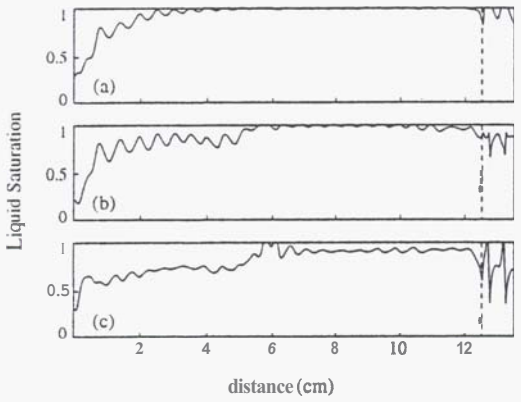

Figure 7. Experiment B. Three (normalized) images of liquid saturation: image (a) was taken within 0.5 seconds of initiation of boiling, image (b) 0.5 seconds later, and image (c) approximately 8 minutes later.

Figure 7 (a) shows the initiation of a boiling front from the depressurized end. Boiling appears to also have begun at the closed end of the core even before the boiling front reaches this end. A small amount of water lies between the rock and the plastic endcap which seals this closed end. It is this "end water" which appears to begin to boil almost immediately (see portion of scan to the right of dotted line in Figure 7). In Figure 7 (b) the progression of the boiling front can be seen as well as the continuation of boiling in the water at the end of the core. Over time, some boiling occurs throughout the core [see Figure 7 (c)].

Further observations (not shown here) indicate increases in saturation at some regions at later times. Such an increase may be due to recondensation of moving steam or to the flow of water back into the core. Upon removal of the core from the NMR, it was noted that the core felt cold to the touch. A qualitative deduction, then, is that the core was too cold for further boiling to take place under the conditions of the experiment.

The speed at which the boiling front moves through the core in Experiments B is closer to numerical estimates, but because the core is finite, the predictions of the semi-infinite model may not apply.

5. BOILING IN POROUS MEDIA: COMPUTER SIMULATIONS

Several simulations using HYDROTHERM (Hayba & Ingebritsen, 1994) were carried out for comparison with both the finite core experiments and similarity solutions (SP flow only). Unfortunately pressures are constrained in HYDROTHERM to be no less than 0.5 bar so comparisons with the physical experiments are qualitative only.

Simulations were carried out on a one-dimensional core of length 14.5 cm, ρ_r = 2000 kg/m^3, ϕ = 0.18, K = 2 W/mK, c_r = 1000 J/kg, and $k = 10^{-12}$ m^2. The core was assumed to be initially saturated with liquid water, at a pressure $p_{initial}$ = 1.1 bar and temperature $T = T_{sat}(p)$ = 102.3 °C. Constant temperature and pressure conditions of p = 1 bar and $T = T_{sat}(p)$ = 99.6 °C were placed on the depressurized end.

When no-flow boundary conditions were placed on the end opposite that which was depressurized, a boiling front was initiated at the depressurized end and progressed through the porous medium [see Figure 8 (a)]. As the system approached thermodynamic equilibrium, increases in liquid saturation were seen [see Figure 8 (b)]. Calculated velocities indicated that water was flowing back into the core replenishing the depleted zone. Such late-time increases in liquid saturation indicate consistency in this aspect of the simulations and physical experiments. In the physical experiment this had a cooling effect on the region. In the event that such an effect were produced in hydrothermal eruptions, it would slow the eruption in progress, and any cooling effect on the area may explain long recovery times between subsequent eruptions.

When "end-water" was placed at the closed end of the porous medium, small-scale boiling was indicated almost immediately in this water (not shown). This boiling, however, occurred in very small quantities in the simulations, much smaller than the NMR profiles indicated.

Good agreement between the simulation and the similarity solution was obtained up to the time at which the boiling front had progressed completely through the core. Late-time saturation increases are a feature of the finiteness of the core and are therefore not predicted by the similarity solution.

When constant temperature and pressure boundary conditions were placed on the end opposite that which was depressurized, we again saw the progression of a boiling front through the porous medium [see Figure 9 (a)]. As this boiling front moves through the core, heat was removed from the system [see Figure 9 (d), t < 20 s]. Once the boiling front had progressed completely through the porous medium, increases in liquid saturation were again seen, but water velocities indicate in this case these were due to water being fed from the end opposite that which was depressurized. A liquid-resaturation front moved back through the core until the system eventually reached a steady state [see Figure 9(b)]. Comparisons in this case cannot be made with the NMR experiment as the physical experimental system was closed at one end.

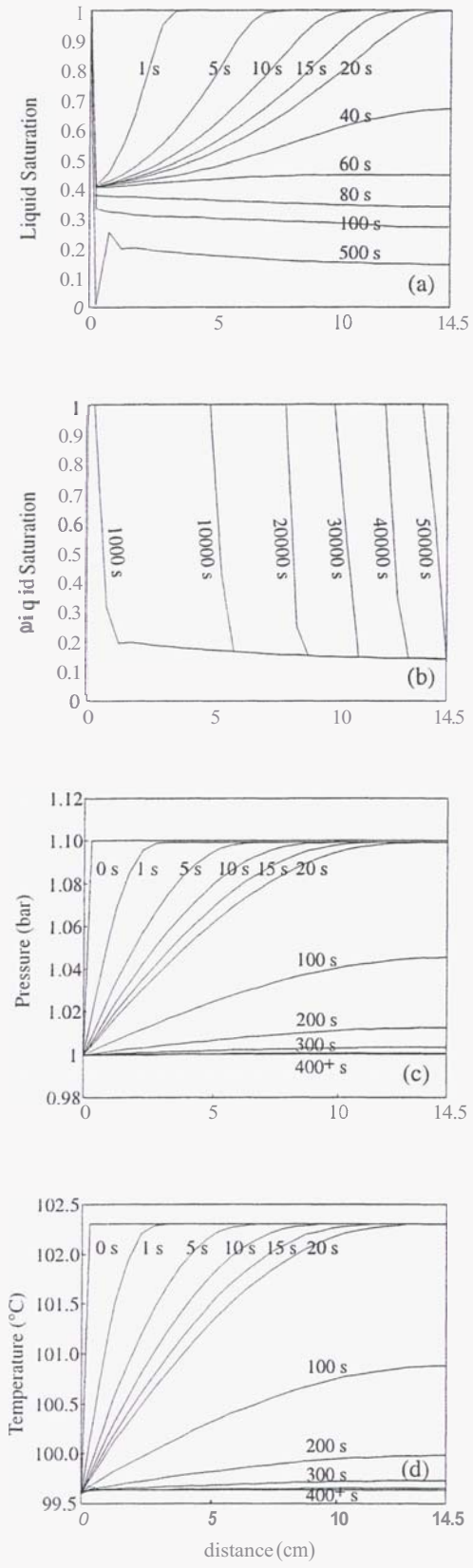

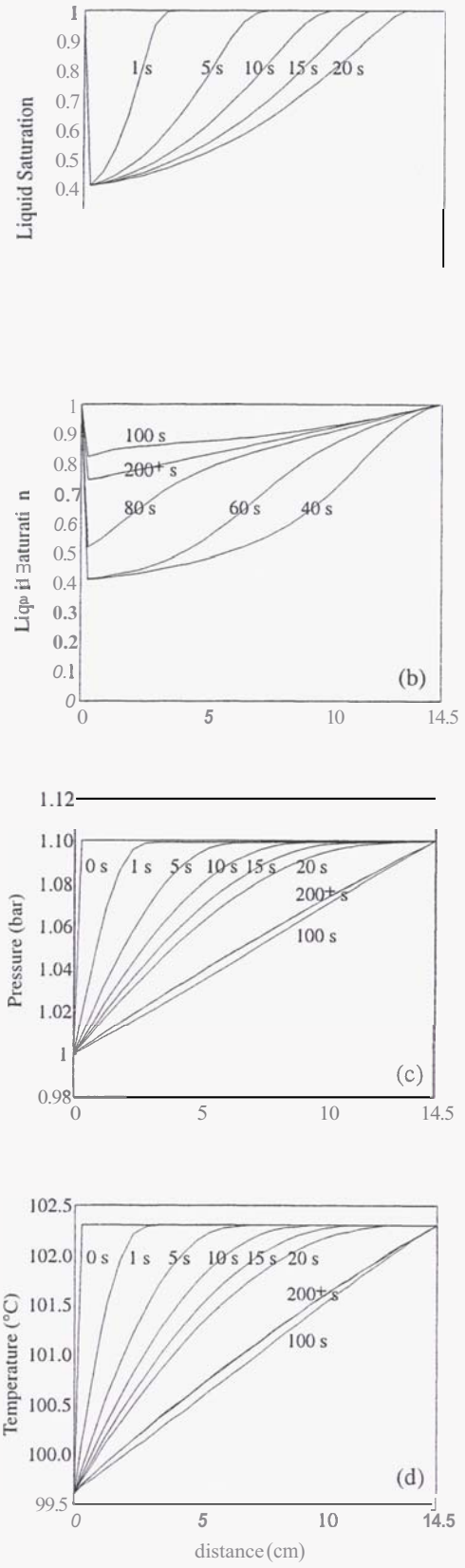

Figure 8. Saturation, pressure and temperature curves for one-dimensional core. Constant pressure and temperature conditions at $x = 0$ cm, no flow boundary conditions at $x = 14.5$ cm. (See text for details.)

Figure 9. Saturation, pressure and temperature curves for one-dimensional core. Constant pressure and temperature conditions at both ends. (See text for details.)

Good agreement between the simulation and the similarity solution was again obtained up to the time at which the boiling front has progressed completely through the core.

6. SUMMARY AND CONCLUSIONS

Numerical and physical experiments were conducted to investigate some aspects of transient boiling processes in porous media. The construction of a laboratory hydrothermal eruption confirmed the possibility that an eruption could be triggered by a pressure reduction and that a boiling front could be initiated at one end of a porous medium.

A one-dimensional semi-infinite mathematical model was solved and results compared with physical experimental data. Because physical experiments were constrained to be finite, direct comparison of all aspects of results was not possible. Both numerical and physical experiments show a boiling front initiated at one end of the porous medium. However, the rate at which the front progressed through the core and boiling effects at the closed end of the core appear to be features of the finiteness of the physical experiment which were not predicted by the semi-infinite model.

Both experimental and mathematical models are being modified in order to achieve consistency. It is hoped that improved models of this transient boiling process will further help the understanding of the physical mechanisms which drive hydrothermal eruptions.

ACKNOWLEDGMENTS

The physical experiment detailed in Section 4 was done with funds provided by the Massey University Research Fund, the contribution of which is gratefully appreciated. Thanks are also due to Sarah Codd for her assistance with the NMR experiments and interpretation.

REFERENCES

Allis, R.A. **(1984).** ***The 9 April 1983 Steam Eruption at Craters of the Moon Thermal Area, Wairakei.*** DSIR Geophysics Division Report No. **196.**

Hayba, D.O. and Ingebritsen, S.E. **(1994).** The Computer Model HYDROTHERM, A ***Three-Dimensional Finite-Difference Model to Simulate Ground-Water Flow*** *and* ***Heat Transport in the Temperature Range of 0 to*** *1,200°C.* U.S. Geological Survey Water-Resources Investigations Report 94-4045, 85p.

Smith, **T.A.** and McKibbin, R. **(1997).** Modelling of Hydrothermal Eruptions: A Review. Proc. ***19th NZ Geothermal Workshop 1997.*** University of Auckland, pp. **123-128.**

Smith, **T.A.** and McKibbin, R. **(1998).** Towards a Hydrothermal Eruption Flow Model. Proc. ***20th NZ Geothermal Workshop 1998,*** University of Auckland, pp.**387-392.**
1109-1130.